Stanley, J., Flowers, R. M. (2016): Dating kimberlite emplacement with zircon and perovskite (U-Th)/He geochronology. - *Geochemistry Geophysics Geosystems (G3)*, *17*, 11, pp. 4517—4533.

DOI: http://doi.org/10.1002/2016GC006519

AGU PUBLICATIONS

Geochemistry, Geophysics, Geosystems

RESEARCH ARTICLE
10.1002/2016GC006519

Dating kimberlite emplacement with zircon and perovskite (U-Th)/He geochronology

Jessica R. Stanley[1,2] and Rebecca M. Flowers[1]

[1]Department of Geological Sciences, University of Colorado Boulder, Boulder, Colorado, USA, [2]Now at GFZ-German Research Centre for Geosciences, Telegrafenberg, Potsdam, Germany

Key Points:
- Sixteen southern African kimberlites were dated using zircon and/or perovskite (U-Th)/He geochronology
- (U-Th)/He of xenocrystic zircon can date kimberlite eruption if zircon are reset during eruption or resided at >200°C prior to entrainment
- Perovskite (U-Th)/He is effective for kimberlite dating and has a higher He closure temperature than zircon

Supporting Information:
- Supporting Information S1
- Table S1
- Table S2

Correspondence to:
J. R. Stanley,
jessica.stanley@colorado.edu

Citation:
Stanley, J. R., and R. M. Flowers (2016), Dating kimberlite emplacement with zircon and perovskite (U-Th)/He geochronology, *Geochem. Geophys. Geosyst.*, *17*, 4517–4533, doi:10.1002/2016GC006519.

Received 7 JUL 2016
Accepted 24 OCT 2016
Accepted article online 27 OCT 2016
Published online 16 NOV 2016

Abstract Kimberlites provide rich information about the composition and evolution of cratonic lithosphere. Accurate geochronology of these eruptions is key for discerning spatiotemporal trends in lithospheric evolution, but kimberlites can sometimes be difficult to date with available methods. We explored whether (U-Th)/He dating of zircon and perovskite can serve as reliable techniques for determining kimberlite emplacement ages. We obtained zircon and/or perovskite (U-Th)/He (ZHe, PHe) dates from 16 southern African kimberlites. Most samples with abundant zircon yielded reproducible ZHe dates (≤15% dispersion) that are in good agreement with published eruption ages. The majority of dated zircons were xenocrystic. Zircons with reproducible dates were fully reset during eruption or resided at temperatures above the ZHe closure temperature prior to entrainment in the kimberlite magma. Not dating hazy and radiation damaged grains can help avoid anomalous results for more shallowly sourced zircons that underwent incomplete damage annealing and/or partial He loss during the eruptive process. All seven kimberlites dated with PHe yielded reproducible (≤15% dispersion) and reasonable results. We conducted two preliminary perovskite ^{4}He diffusion experiments, which suggest a PHe closure temperature of >300°C. Perovskite in kimberlites is unlikely to be xenocrystic and its relatively high temperature sensitivity suggests that PHe dates will typically record emplacement rather than postemplacement processes. ZHe and PHe geochronology can effectively date kimberlite emplacement and provide useful complements to existing techniques.

1. Introduction

Kimberlites are small volume, volatile-rich ultramafic rocks derived from mantle depths. They are common in cratonic regions and are the most significant source of the world's diamonds. Kimberlites can entrain xenoliths and xenocrysts from the entire lithospheric column as they transit rapidly to the surface, thereby providing invaluable constraints on the thermochemical character and evolution of the lithospheric mantle [e.g., *Bell et al.*, 2003; *Griffin*, 2003; *Kobussen et al.*, 2008; *Janney et al.*, 2010]. Their low-temperature cooling histories and crustal xenoliths can also be used to constrain cratonic erosion and evaluate the links between surface and deeper processes [*Stanley et al.*, 2013, 2015]. Numerous mechanisms have been proposed for kimberlite genesis, including mantle plume activity and hotspot tracks [e.g., *Le Roex*, 1986; *Skinner*, 1989; *Heaman and Kjarsgaard*, 2000; *Chalapathi Rao et al.*, 2015], tectonically triggered thermal events involving continental break up and lithospheric-scale faults [e.g., *Jelsma et al.*, 2004, 2009; *Moore et al.*, 2008; *Tappe et al.*, 2014, 2016], deep-seated subduction [e.g., *Helmstaedt and Gurney*, 1984; *McCandless*, 1999; *Currie and Beaumont*, 2011; *Duke et al.*, 2014], and/or some combination of these [e.g., *Heaman et al.*, 2004]. Others have argued that kimberlite volcanism is triggered from the edges of large, low seismic velocity structures in the deep mantle [*Torsvik et al.*, 2010] and used the ages and locations of kimberlite eruptions to support the longevity of these mantle structures and calibrate plate motion reconstructions [*Torsvik et al.*, 2014]. Accurate emplacement ages therefore provide essential information both for interpreting kimberlite mantle xenolith suites and deciphering spatiotemporal patterns of kimberlite eruptions to evaluate models for their origins.

For these reasons, much attention has focused on approaches to reliably date kimberlites. However, in some circumstances, it remains surprisingly difficult to obtain accurate and reproducible kimberlite eruption dates. Early approaches to kimberlite dating included phlogopite-whole rock Rb-Sr isochrons and phlogopite ^{40}Ar-^{39}Ar dating, but these results can be complicated by initial isotopic heterogeneity and postemplacement sample alteration [e.g., *Allsopp and Barrett*, 1975; *Brown et al.*, 1989; *Phillips et al.*, 1999]. Zircon U-

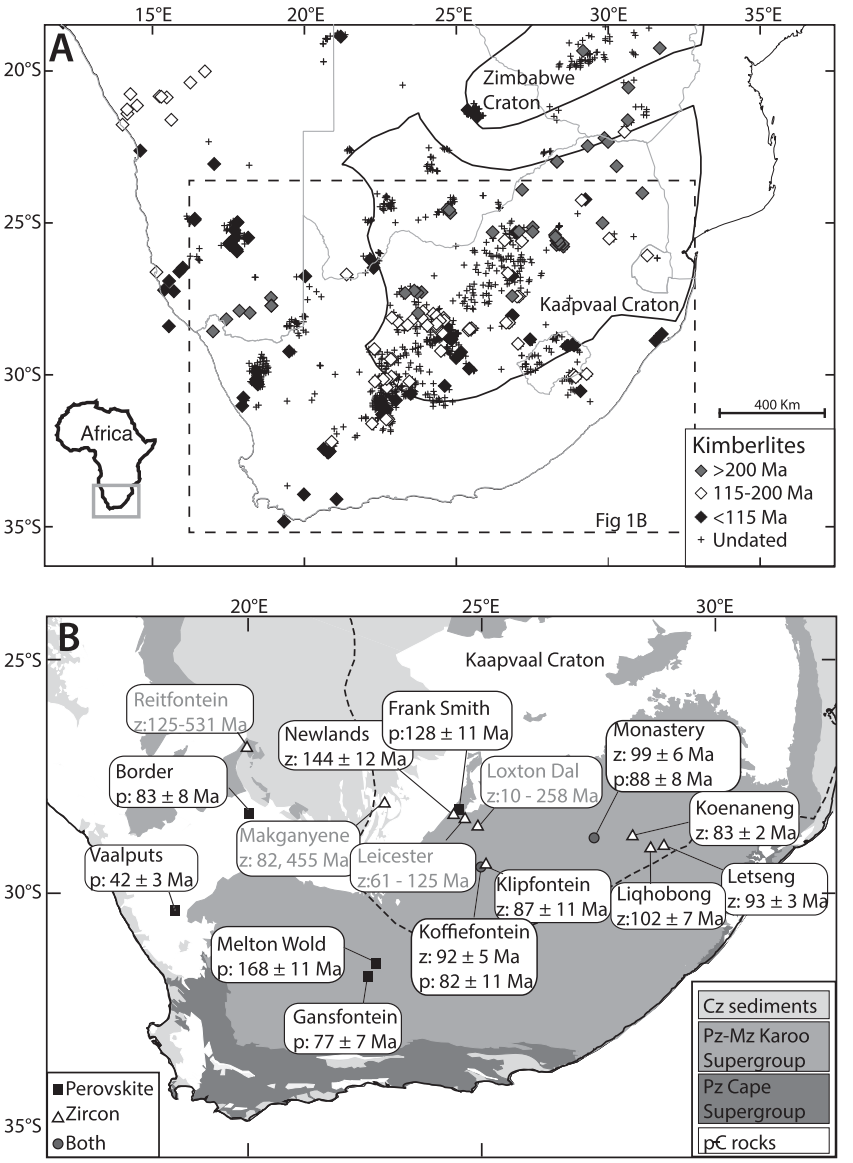

Figure 1. (a) Map of southern Africa with kimberlite locations and craton outlines. Kimberlite age database from *Jelsma et al.* [2009]. (b) Simplified geologic map with sample locations, ZHe dates, and PHe dates. Samples with gray text yielded few zircon and scattered ZHe dates.

Pb dating is an alternative, but in some cases the results appear to predate the actual kimberlite emplacement age by 5–40 Ma, presumably due to zircon growth prior to eruption [*LeCheminant et al.*, 1998; *Moore and Belousova*, 2005]. This pattern has led some authors to disregard zircon U-Pb dates in kimberlite age compilations [*Moore et al.*, 2008]. Fission track dating of kimberlitic zircons [*Haggerty et al.*, 1983] and rutile U-Pb dating [*Tappe et al.*, 2014] have been successful in several cases but are not extensively applied.

Perovskite U-Pb dating is now the most widely employed kimberlite dating tool because perovskite is a common kimberlite phase that crystallizes from the host magma, can contain high U and Th, and is relatively unsusceptible to alteration [e.g., *Kramers and Smith*, 1983; *Heaman*, 1989; *Wu et al.*, 2010; *Tappe and Simonetti*, 2012; *Griffin et al.*, 2014; *Sarkar et al.*, 2015]. However, even this technique has its limitations, which vary based on the analytical approach used. Perovskite can contain appreciable common Pb that reduces the precision and accuracy of U-Pb dates. This is particularly true for time-effective and cost-effective in situ laser ablation (LA)-ICP-MS analyses. These data rely on the ^{207}Pb method of correcting for common Pb, which assumes the mineral does not contain multiple age domains and is concordant

[*Cox and Wilton*, 2006]. New SIMS calibration protocols allow internal assessment of isotopic concordance and common Pb correction by the ^{204}Pb method, which yields more precise in situ dates [*Li et al*., 2010]. U-Pb analysis of perovskite by TIMS can yield high-precision data but is analytically time intensive and costly. Additionally, some kimberlites contain multiple perovskite age populations such that it is difficult to interpret which represents the eruption age [*Heaman*, 1989; *Griffin et al*., 2011, 2014].

Developing new kimberlite dating methods is worthwhile to complement these existing techniques. The middle temperature (~150–400°C) geochronometers of the (U-Th)/He system have the potential to avoid some of the challenges outlined above. Many (U-Th)/He thermochronologic applications are aimed at deciphering the cooling history of rocks during exhumation [e.g., *Ehlers*, 2005; *Reiners and Shuster*, 2009], but for fast-cooled volcanic rocks the cooling date may be equivalent to the eruption age [e.g., *Tagami et al*., 2003; *Blondes et al*., 2007; *Blackburn et al*., 2008]. Previous (U-Th)/He study of multiple phases (zircon, titanite, magnetite, garnet, and apatite) from several kimberlites in Kansas showed that He dating of kimberlites has promise, although the results were characterized by variable age dispersion [*Blackburn et al*., 2008]. ZHe data were obtained for two kimberlite samples, with results for one sample dating and the other postdating kimberlite emplacement [*Blackburn et al*., 2008]. The apatite dates were substantially younger than eruption [*Blackburn et al*., 2008], as might be expected because apatite's lower temperature sensitivity (<90°C) makes it more likely to record to posteruption erosion events [e.g., *Stanley et al*., 2013]. The mean titanite, magnetite, and garnet (U-Th)/He dates for several of the Kansas kimberlites approximated the kimberlite emplacement age, but in some cases the individual He dates were highly dispersed (up to 26% dispersion) [*Blackburn et al*., 2008].

Here we focus specifically on whether (U-Th)/He geochronology of two minerals, zircon and perovskite, can reliably date kimberlite eruption. We targeted zircon because its He diffusion kinetics are well studied [*Reiners*, 2005; *Guenthner et al*., 2013], it generally has relatively high U-Th concentrations (100s to 1000s ppm), and it appeared the most promising of the phases dated by *Blackburn et al*. [2008]. Typical zircon is characterized by a temperature sensitivity high enough (~150–200°C) that this mineral should not be perturbed by postemplacement surface processes, although substantial radiation damage accumulation can lower its He retentivity [*Guenthner et al*., 2013]. Xenocrystic zircons can record the emplacement age if they were heated sufficiently during eruption to cause complete He loss, thereby resetting the (U-Th)/He system, or if they resided at temperatures above the ZHe closure temperature prior to incorporation into the kimberlite magma. We targeted perovskite because it is a common groundmass phase in kimberlites, crystallizes directly from the magma, and typically contains appreciable U and Th. We are unaware of any previous He dating or diffusion kinetic work on perovskite. Southern Africa has one of the most widely dated kimberlite suites globally, making it an ideal location to test the ZHe and PHe systems on kimberlites that have been dated by a variety of other techniques (Figure 1). Here we present ZHe and PHe data for a set of South African kimberlites, along with perovskite ^{4}He diffusion experiment data, to evaluate the effectiveness of these systems as kimberlite geochronometers.

2. Background and Samples

2.1. (U-Th)/He Geochronology

(U-Th)/He geochronology is based on the radioactive decay of trace U, Th, and to a lesser extent Sm to ^{4}He in a mineral's structure. At high temperatures He escapes rapidly from the crystal, while at low temperatures it is quantitatively retained. The temperatures at which He is lost or retained depend on the mineral's He diffusion kinetics. In some minerals, radiation damage accumulation can increase or decrease the He retentivity depending on damage level [*Shuster et al*., 2006; *Flowers et al*., 2009; *Gautheron et al*., 2009; *Guenthner et al*., 2013]. In zircon, initial damage accumulation causes the He closure temperature to increase from about 140 to 220°C, while at still higher damage the closure temperature drops to <50°C [*Guenthner et al*., 2013]. For protracted thermal histories, the effect of radiation damage may appear as a correlation between date and eU, where eU is effective uranium, a proxy for radiation damage (eU = U + 0.235Th) [*Flowers et al*., 2007]. Date-eU plots are useful for evaluating the possible influence of radiation damage and thermal history on the results [e.g., *Flowers et al*., 2009; *Guenthner et al*., 2013] and can be exploited to decipher additional thermal history information [e.g., *Flowers and Kelley*, 2011]. Radiation damage can be annealed by heating, which for zircon and apatite generally occurs at higher temperatures than those that cause He loss [e.g., *Flowers et al*., 2009; *Shuster and Farley*, 2009; *Guenthner et al*., 2013]. The grain size and fragmentation of the dated mineral can also affect the (U-Th)/He date [*Reiners and Farley*, 2001; *Brown et al*., 2013], although

these factors are less significant than radiation damage. These various effects should not be substantial for relatively young (<200 Ma) and rapidly cooled samples like those of our study.

During U and Th decay, ^{4}He atoms are released with sufficient energy such that they travel up to ~20 μm away from their parent nuclide. A geometric correction is applied to account for the He that is lost by ejection from the crystal rather than by diffusion (the α-ejection correction) [*Farley et al*., 1996]. The magnitude of this correction increases for smaller grain sizes, which increases the uncertainty on the date.

Sample (U-Th)/He data dispersion is commonly 10–15%. Some of this variability is due to the kinetic factors and α-ejection correction uncertainties described above. However, additional effects such as parent isotope zonation [e.g., *Farley et al*., 2011; *Ault and Flowers*, 2012; *Johnstone et al*., 2013] and He implantation from outside the grain [e.g., *Spiegel et al*., 2009; *Gautheron et al*., 2012] may also contribute.

2.2. Southern African Kimberlite Samples

Southern Africa has >1000 known kimberlite bodies, including the type locality for kimberlite (Figure 1a). Of these, > 200 have been dated and range in age from >1600 Ma to ~50 Ma. These kimberlites intrude through the southern African shield, which is made up of the Archean Kaapvaal and Zimbabwe cratons surrounded by Proterozoic mobile belts. The Precambrian rocks are covered in places by the ~300–180 Ma Karoo sedimentary sequence, the ~183 Ma Karoo large igneous province, and Cenozoic sedimentary rocks (Figure 1b). Because of their abundance and significance to the diamond industry, southern African kimberlites and their mantle xenoliths have played a prominent role in our understanding of cratonic growth, stability, metasomatism, and modification. Two major Jurassic to Cretaceous kimberlite suites are particularly well studied: the ~200–110 Ma Group 2 kimberlites and the ~100–70 Ma Group 1 kimberlites [e.g., *Moore et al*., 2008; *Jelsma et al*., 2009; *Griffin et al*., 2014].

We targeted 23 Cretaceous kimberlites from a wide geographic region in South Africa including localities both on and off the Kaapvaal craton. The postemplacement cooling history of most of these kimberlites is well constrained by our previous apatite (U-Th)/He work on the same and nearby kimberlite samples [*Stanley et al*., 2013, 2015]. The samples were collected at the kimberlite itself or obtained from the large Mantle Room collection at the University of Cape Town. Following mineral separation, we ultimately dated 16 of these samples by ZHe and/or PHe geochronology (Figure 1b). Table 1 provides a summary of information about the dated kimberlites. Eleven have previously published ages ranging from ~165 to ~85 Ma based on mica-whole-rock Rb-Sr isochrons, perovskite U-Pb, and/or zircon U-Pb. We also studied five undated kimberlites. The kimberlite samples include Group 1 and Group 2 chemical affinities, as well as samples transitional between the two groups and one melilitite (Table 1). Whole rock samples consisted of 2–5 kg of diatreme and hypabyssal facies kimberlite. We specifically attempted to avoid large crustal inclusions because zircons within large xenoliths may have been insulated during eruption and potentially not heated sufficiently to reset the (U-Th)/He system.

3. Methods

3.1. (U-Th)/He Methods

Zircon and perovskite crystals were separated using standard density and magnetic separation techniques. Individual grains were selected for (U-Th)/He analysis based on crystal form and size. Grains with a minimum dimension ≥60 μm were selected to minimize the magnitude of the α-ejection correction. If multiple populations of zircon appeared to be present, care was taken to avoid damaged, cracked, hazy or brown zircon because grains with these characteristics are commonly metamict. Samples selected for PHe analysis were confirmed to have perovskite by examining the EDS spectra of representative grains on the JOEL 8600 electron microprobe at the University of Colorado.

Grain shapes and dimensions were measured from photographed grains prior to loading in Nb packets for analysis. Helium measurements were made on an ASI Alphachron at the University of Colorado Boulder (CU). The packets containing the grains were lased under vacuum to extract the radiogenic ^{4}He. All zircon and the first subset of perovskite were lased at 15 A for 10 min, while the second subset of perovskite grains was lased at 10 A for 10 min. Gas was spiked with ^{3}He, purified using gettering methods, and measured on a quadrupole mass spectrometer. This was repeated at least once per grain to ensure all gas was removed from the grain.

Table 1. Summary of Studied Kimberlites and Melilitite

Kimberlite	Lattitude (°S)	Longitude (°E)	Elevation (m)	Group[a]	Published Age(s) (Ma)[b]
Border	28.23995	19.98375	820	1[1]	No published age
Frank Smith	28.2457	24.5151	1091	1[2]	114 ± 1, Rb-Sr, *Smith et al.* [1985]
Gansfontein	31.77808	22.56479	1510	1[3]	No published age
Klipfontein	29.396	24.981	1199	1[4]	97 ± 1, U-Pb perovskite, *Griffin et al.* [2014]
Koenaneng	28.79123	28.19901	1662	1[5]	No published age
Koffiefontein	29.4268	24.9925	1196	1[6]	90.4 Ma, U-Pb zircon, *Davis* [1977], 100 ± 2, U-Pb perovskite, *Griffin et al.* [2014]
Leicester	28.3708	24.6528	1156	Tr[7]	93 ± 1, U-Pb perovskite, *Griffin et al.* [2014], 93.6, U-Pb zircon *Davis* [1977]
Letseng	29.00359	28.86751	3051	1[8]	94.6, U-Pb zircon, *Allsopp et al.* [1989]
Liqhobong	28.98906	28.61115	2545	1[3]	91.2 ± 1, U-Pb perovskite, *Griffin et al.* [2014]
Loxtondal	28.61198	24.9124	1236	2[9]	No published age
Makganyene	22.15282	22.91818	1280	2[10]	121 ± 0.5, Rb-Sr *Brown et al.* [1989]
Melton Wold	31.49735	22.74579	1331	Tr[11]/2[3]	163 ± 2, U-Pb perovskite, *Griffin et al.* [2014]; 143 ± 7, U-Pb perovskite, *Smith et al.* [1994]
Monastery	28.810833	27.42195	1629	1[2]	88.6 ± 1, U-Pb perovskite, *Batumike et al.* [2008]; 88 ± 2, Rb-Sr, *Allsopp and Barrett* [1975]; 90.4, U-Pb zircon, *Davis* [1977]
Newlands	28.3506	24.3981	1036	2[2]	114 ± 1, Rb-Sr, *Smith et al.* [1985]
Rietfontein	26.74332	20.03708	835	1[12]	71.9 Ma, U-Pb zircon, *Davis* [1977]; 135 ± 4.5 Ma, U-Pb perovskite, *Griffin et al.* [2014]
Melilitite near Vaalputs	30.09814	18.46446	1002	mel[13]	No published age

[a]Group denotes chemical affinity 1: Group 1, 2: Group 2, Tr: transitional, mel: melilitite. References for group categorization are [1]*Jelsma et al.* [2004] by association with the Ariamsvlei Cluster, [2]*Smith et al.* [1983], [3]*Nowell et al.* [2004], [4]*Griffin et al.* [2014], [5]by association with other Lesotho kimberlites and description in *Dawson* [1962], [6]*Becker and Le Roex* [2006], [7]*Becker et al.* [2007], [8]*Woodhead et al.* [2009], [9]*Field et al.* [2008], [10]*Brown et al.* [1989], [11]*Skinner et al.* [1992], [12]*Appleyard et al.* [2007], and [13]*Moore and Verwoerd* [1985] by association with the Namaqualand Bushmanland group.

[b]Uncertainty on published ages is 1σ, when provided (U-Pb zircon dates have no published uncertainty).

The packets containing the grains were retrieved, placed in Teflon vials, spiked with a ^{235}U, ^{230}Th, and ^{145}Nd tracer, and dissolved in 29 *M* HF at 220°C for 72 h in pressure vessels. Samples were then dried and dissolved in 6 *M* HCl for 48 h at 200°C in pressure vessels. The zircon and first subset of perovskite were then dried down, taken up in a mixture of 175 μL of HNO_3 and 25 μL of HF, and diluted with 2.8 mL or more of water. The second subset of perovskite was taken up in a mixture of 175 μL of HNO_3 and 50 μL of HF and diluted with 2.8 mL of water. A Thermo-Finnigan Element2 sector field ICPMS at CU was used to measure U and Th for all dissolved samples. Sm was additionally measured for dissolved perovskites. Sm was not measured for zircon because of its minimal concentration in zircon and negligible influence on ZHe dates.

All dated zircon were prismatic crystals, either whole or with one or both tips cleanly broken. We therefore used the tetrahedral prism α-ejection correction of *Ketcham et al.* [2011] for all zircon. Dated perovskite included both fragments and crystals with several different geometries. Perovskite is a mineral with pseudo-cubic habit, and dated geometries included cubes, octahedrons, and dodecahedrons. For perovskite grains showing crystal faces, an α-ejection correction was calculated using the average stopping distance, the grain geometry, and the measured dimensions of each grain using the software by *Gautheron and Tassan-Got* [2010]. The results were then cross-checked with the geometries of *Ketcham* [2011]. A modified correction was used if broken crystal faces were observed (Table 3) [*Gautheron and Tassan-Got*, 2010]. We computed the stopping distances for each alpha particle in the decay chain of ^{238}U, ^{235}U, and ^{232}Th (average stopping distance for each chain 15.9, 18.5, and 18.8 μm, respectively, supporting information Table S1) using the SRIM software (Stopping Ranges of Ions in Matter, www.srim.org) [*Ziegler et al.*, 2010]. We then combined this result with the Th/U of each dated grain to calculate its average stopping distance. No α-ejection correction was applied to the fragments lacking obvious crystal faces because grain fragmentation likely occurred during sample processing. Most of the dated fragments were relatively large, wedge

shaped shards with conchoidal surfaces, which we assume did not reside close enough to the original crystal face to suffer significant He loss by α-ejection. However, if this assumption is not valid it could contribute to variability in the sample dates.

3.2. ^{4}He Step-Heating Diffusion Experiment Methods

Perovskite has not previously been used for (U-Th)/He geochronology and understanding its temperature sensitivity is important for interpreting the significance of PHe dates. Our primary goal with these preliminary diffusion experiments was to establish whether the perovskite closure temperature is high enough that the PHe dates for these quickly cooled samples record eruption rather than posteruption processes. We performed two stepwise degassing ^{4}He diffusion experiments on single grain fragments from the Melton Wold kimberlite (sample SA11-33A). This sample was selected because it has previously published U-Pb perovskite dates and the perovskite grains in the sample were dominated by large, cleanly broken fragments. The individual grains were chosen based on size and the presence of smooth, conchoidally fractured crystal faces. The selected grains were similar to the dated fragments and had equivalent spherical radii of 81 and 45 μm. In each experiment a perovskite fragment was loaded in a Nb tube, placed in the diffusion cell of the ASI Alphachron at CU, and heated using a light bulb heating apparatus [*Farley et al*., 1999]. Each grain was heated to temperatures of 150–600°C and held isothermally for periods of 30–240 min in a series of prograde, retrograde, and final prograde steps. The released gas volume was spiked with ^{3}He, purified, and measured using a quadruple mass spectrometer. After the heating schedule was complete, samples were fully degassed by laser heating to measure the remaining fraction of gas. The perovskite was then retrieved, dissolved, and its U, Th, and Sm measured following the methods described in section 2.2 to enable determination of its (U-Th)/He date. The full heating schedule and data table are in supporting information Table S2. Diffusion parameters were calculated using the fraction of gas released, the holding time, and assuming a spherical geometry with the method of *Fechtig and Kalbitzer* [1966].

4. Results

4.1. ZHe Results

Of the 23 kimberlites that we separated as part of this study, 13 yielded zircon. We selected 11 of these samples for ZHe dating based on a range of zircon quality, with preference given to those kimberlites with independent age constraints. Of these 11 samples, eight yielded abundant zircon and three did not. We analyzed five to six single-grain analyses per sample for those with abundant zircon, and were only able to acquire two to four analyses per sample for those with little yield, for a total of 50 ZHe dates. All data are reported in Table 2. The 1σ analytical uncertainty for the individual grain dates includes the uncertainties in U, Th, He and grain length measurements. Six of the eight samples with abundant zircon yielded reproducible ZHe dates with $\leq$15% sample standard deviation (1σ) and average dates from $\sim$83 Ma to $\sim$144 Ma (Table 2). In a seventh sample, Koenaneng, four grains yielded dates from 80 to 85 Ma with two grains $>$200 Ma that were excluded from the sample mean (discussed further in sections 5.1 and 5.2). The eighth sample with abundant zircon, Rietfontein, yielded scattered dates between 125 and 531 Ma. None of the three samples with limited zircon gave reproducible results (36–97% dispersion; Table 2). Figure 1b lists the mean sample date and 1σ deviation for samples with $\leq$15% dispersion, and the range in individual grain dates for those with $>$15% dispersion. Supporting information Figure S1 shows ZHe date-eU plots for all samples. None of the reproducible samples have clear date-eU patterns. The other samples are discussed in more detail below.

4.2. PHe Results

Of the 19 kimberlites examined, 11 contained perovskite grains with minimum dimension $>$50 μm. Additional samples may have yielded perovskite in the smaller grain size or more magnetic fractions of the mineral separates that we did not inspect. We selected seven of these samples for PHe dating based on existing age constraints and perovskite grain size. Two of these samples are among those for which we also acquired ZHe dates. The 64 individual grain PHe dates from these seven kimberlite samples are reported in Table 3 and supporting information Table S3, the means and uncertainties are shown on Figure 1b, and PHe date-U and PHe date-Th plots for all samples are included in Figure 2 and supporting information Figure S2. Uncertainties for perovskite are reported in the same manner as for zircon.

Table 2. Zircon (U-Th)/He Data From Southern African Kimberlites

Sample	Mass (μg)	r[a] (μm)	Ft[b]	U (ppm)	Th (ppm)	eU[c] (ppm)	Th/U	He (ncc)	Raw Date (Ma)	Corr Date (Ma)	1σ[d] (Ma)
Reproducible Samples (≤15% Dispersion)[e]											
					SA12-4: Klipfontein-07 Kimberlite						
z1	3.2	42	0.73	161.6	41.5	171.4	0.26	3.7	55	75	0.6
z2	5.9	50	0.77	76.4	17.3	80.5	0.23	3.6	63	82	0.9
z3	5.1	47	0.77	71.8	27.1	78.2	0.38	3.6	75	98	1.6
z5	3.6	45	0.75	70.0	20.3	74.8	0.29	1.9	58	78	1.2
z6	2.2	40	0.72	64.5	50.3	76.3	0.78	1.5	75	104	1.9
Mean[f]: 87 ± 12.7 Ma, 15% deviation											
Published age: 97 ± 1, U-Pb perovskite, *Griffin et al.* [2014]											
					SA12-20A: Koenaneng Kimberlite						
z1	4.9	47	0.76	86.5	37.5	95.3	0.43	3.6	64	85	0.8
z2	4.8	50	0.78	95.9	53.1	108.4	0.55	4.2	66	85	1.0
z3	*3.8*	*45*	*0.75*	*257.4*	*88.8*	*278.3*	*0.35*	*21.2*	*164*	*219*	*2.1*
z4	3.7	44	0.74	211.6	40.6	221.2	0.19	6.0	60	81	1.1
z5	8.5	58	0.81	154.4	54.8	167.2	0.36	11.3	66	81	0.9
z6	*5.0*	*46*	*0.76*	*120.7*	*74.4*	*138.2*	*0.62*	*16.1*	*191*	*251*	*5.2*
Mean: 83 ± 2.3 Ma, 3% deviation (excluding z3, z6)											
No published age for this locality											
					SA12-3: Koffiefontein Kimberlite						
z1	4.4	47	0.76	1050.2	56.2	1063.4	0.05	42.8	75	99	0.7
z3	2.7	43	0.76	2209.3	135.0	2241.0	0.06	50.6	69	91	0.6
z3	3.7	46	0.75	965.0	40.7	974.6	0.04	26.9	62	82	0.6
z4	1.7	39	0.71	194.3	180.4	236.7	0.93	3.3	66	93	0.8
z5	2.4	44	0.75	2068.6	105.5	2093.4	0.05	42.4	70	93	1.0
Mean: 92 ± 6.0 Ma, 7% deviation											
Published age: 90.4, U-Pb zircon, *Davis et al.* [1977]											
					SA12-24A: Letseng-la-terai Kimberlite						
z1	29.4	87	0.86	237.1	234.5	292.2	0.99	87.2	83	97	0.8
z3	20.9	78	0.86	310.5	250.3	369.3	0.81	72.9	77	90	0.6
z3	22.6	84	0.87	269.2	286.6	336.6	1.06	71.8	78	89	0.6
z4	19.8	74	0.85	226.6	216.6	277.5	0.96	52.4	79	93	1.1
z5	15.2	68	0.84	297.4	341.0	377.5	1.15	55.9	80	96	1.1
Mean: 93 ± 3.1 Ma, 3% deviation											
Published age: 94.6, U-Pb zircon, *Allsopp et al.* [1989]											
					SA12-22B: Liqhobong Kimberlite						
z1	8.9	58	0.80	169.9	45.9	180.7	0.27	16.8	86	108	1.0
z2	12.5	65	0.82	235.7	144.9	269.7	0.61	33.9	82	101	0.7
z3	4.9	47	0.76	125.9	90.5	147.2	0.72	7.4	83	110	0.6
z4	4.7	49	0.77	42.3	26.4	48.5	0.62	2.0	72	95	1.4
z5	1.7	39	0.71	256.7	178.2	298.5	0.69	4.2	70	98	0.8
Mean: 102 ± 6.7, 7% deviation											
No published age for this locality											
					SA11-16A: Monastery Kimberlite						
z1	5.3	49	0.78	173.2	36.0	181.6	0.21	8.9	77	99	0.9
z2	7.9	55	0.80	32.2	17.6	36.3	0.55	2.5	71	88	0.7
z3	12.4	65	0.82	776.4	51.0	788.4	0.07	96.3	81	99	1.0
z6	1.9	58	0.71	305.7	47.7	316.9	0.16	5.3	72	101	0.7
z7	3.6	75	0.76	88.3	47.3	99.5	0.54	3.6	81	106	1.8
Mean: 99 ± 6.6 Ma, 7% deviation											
Published age: 88.6 ± 1.1,U-Pb perovskite, *Batumike et al.* [2008]											
					SA12-6A: Newlands Kimberlite						
z1	9.9	62	0.81	82.9	14.7	86.4	0.18	11.5	110	135	1.3
z2	3.8	46	0.75	61.2	22.1	66.4	0.36	3.4	109	145	1.6
z3	10.5	64	0.82	76.2	13.0	79.2	0.17	11.9	117	143	1.0
z4	23.6	82	0.87	98.7	17.2	102.7	0.17	34.5	117	135	2.2
z5	1.8	39	0.72	60.7	25.2	67	0.42	1.7	118	163	3.5
Mean: 144 ± 11.5 Ma, 8% deviation											
Published age: 114 ± 1 Ma, Rb-Sr mica and whole rock, *Smith et al.* [1985]											
Dispersed Samples (>15% dispersion)[e]											
					SA12-12: Leicester Kimberlite						
z1	298.8	197	0.94	2.2	9.8	4.5	4.45	1.4	58	61	0.6
z2	13.7	71	0.83	2.7	17.9	6.9	6.50	3.9	103	125	6.6
z3	64.6	111	0.89	1.5	10.9	4.1	7.25	1.7	75	84	1.3
					SA13-35: Loxtondal Kimberlite						
z1	5.2	50	0.78	211.5	135.9	243.4	0.64	19.6	127	161	3.1
z2	5.4	54	0.80	112.5	56.6	125.8	0.50	17.3	206	258	3.9
z3	13.3	70	0.84	73.1	193.5	118.5	2.65	14.5	75	90	1.0
z4	3.5	44	0.75	2112.8	5763.2	3467.1	2.73	10.6	7	10	4.9

Table 2. (continued)

Sample	Mass (μg)	r[a] (μm)	Ft[b]	U (ppm)	Th (ppm)	eU[c] (ppm)	Th/U	He (ncc)	Raw Date (Ma)	Corr Date (Ma)	1σ[d] (Ma)
SA13-33: Makganyene Kimberlite											
z1	1.9	37	0.69	115.0	151.8	150.7	1.32	10.8	308.3	445.3	9.1
z2	2.2	39	0.73	232.0	237.9	287.9	1.03	4.6	60.0	82.4	1.2
SA13-30: Rietfontein Kimberlite											
z1	2.6	42	0.74	207.2	28.8	214.0	0.14	10.3	153	207	3.2
z2	1.8	38	0.71	396.1	43.4	406.2	0.11	28.9	320	445	6.7
z3	2.0	41	0.73	164.2	48.1	175.5	0.29	15.3	353	478	9.4
z4	5.1	55	0.79	250.0	92.1	271.7	0.37	23.2	136	172	2.0
z5	1.6	37	0.68	632.4	457.1	739.9	0.72	12.0	86	125	0.7
z6	2.7	45	0.74	276.7	71.1	293.4	0.26	39.3	400	531	4.4

[a]Equivalent spherical radius (r), the radius of a sphere with the same surface area to volume ratio.
[b]Ft is α-ejection correction of *Ketcham et al.* [2011].
[c]eU: effective uranium concentration, weights U and Th for their alpha productivity, computed as [U] + 0.235 × [Th].
[d]Analytical uncertainty based on U, Th, He, and grain length measurements.
[e]Mean dates and uncertainties are reported only for the samples with more than three grains and <15% dispersion.
[f]Mean and 1σ standard deviation of corrected dates. Grains in italics not included in mean.

Our PHe data set consists of two groups of results acquired using slightly different methods. Our first group of PHe dates was obtained using methods identical to those for our zircon grains: 15 A laser power for degassing, and final take-up of the grain in a 1% HF mixture. Supporting information Table S3 reports the data for this first set of analyses. The results for five of the six kimberlites acquired as part of this initial PHe data set are characterized by negative correlations between PHe date and U concentration (gray points, Figures 2a and 2c and supporting information Figures S2A, S2C, and S2G—Frank Smith, Border, Gansfontein, Koffiefontein, and Monastery). Several of these kimberlites also show negative correlations between date and Th concentration (gray points, Figure 2b and supporting information Figures S2D and S2H—Frank Smith, Koffiefontein, and Monastery). Plots of the difference between the individual PHe date and the published kimberlite emplacement age versus U (Figure 2e) and Th (Figure 2f) for all samples display anomalously old dates at lower U and Th concentrations. These relationships are consistent with U and Th loss during measurement or dissolution, because for the same total amount of loss the lower U-Th grains would have greater fractional loss and be more biased toward older dates. U loss by volatilization during degassing has been documented for titanite [*Reiners and Farley*, 1999]. We suspect that U-Th loss occurred either during volatilization or by loss from solution prior to ICPMS analysis.

We therefore obtained a second group of PHe dates for all samples using a modified method: a lower laser power (10 A) for degassing to reduce the likelihood of U and Th volatilization, and a final take-up in 2% HF to ensure no loss of the parent isotopes from solution. All data acquired using this modified method are reported in Table 3. This second group of PHe dates was less dispersed and showed no negative correlations between He date and U or Th concentration (black points, Figure 2, supporting information Figure S2). For example, Figures 2a–2d show that the PHe dates for Frank Smith and Border acquired using this modified method are uniform regardless of U and Th concentration. Similarly, Figures 2e and 2f that summarize the results for all samples show no systematic difference between the published emplacement dates and the PHe results. Given the contrast in the data patterns for the PHe results obtained using these two methods we conclude that our first group of PHe analyses is potentially compromised (supporting information Table S3), but those obtained using our modified perovskite method are reliable (Table 3). We therefore discuss only the results yielded by our second, preferred method for the remainder of the paper.

For six of the seven samples the PHe dates from our preferred method are reproducible at <10% (1σ), with all samples at <15% dispersion (Table 3). Average PHe dates range from 42 to 168 Ma. With the exception of one outlier from Gansfontein (p7, Table 3), the PHe data do not have any of the outliers or highly dispersed results as observed in the ZHe data.

4.3. Perovskite ^{4}He Step-Heating Diffusion Experiment Results

Figure 3 shows the Arrhenius arrays for the two single-crystal ^{4}He diffusion experiments on perovskite from the Melton Wold kimberlite. The initial prograde heating steps of both experiments show an irregular pattern, followed by dominantly linear relationships for the subsequent retrograde and prograde temperature sequences (Figure 3). The complexity of the first prograde sequence shares similarities with the Arrhenius

Table 3. Perovskite (U-Th)/He Data From Southern African Kimberlites and Melilitite for Samples Degassed at 10 A Laser Power

Sample	Mass (μg)	r[a] (μm)	Ft[b]	Grain Geometry[c]	FT Geometry[d]	Broken Faces	U (ppm)	Th (ppm)	Sm (ppm)	eU[e] (ppm)	Th/U	He (ncc)	Raw Date (Ma)	Corr Date (Ma)	1σ[f] (Ma)
SA13-28: Border Kimberlite															
p6	5.1	48	0.74	Octahedra	2-Pyramid tetra	0	54.9	177.7	20.1	96.7	3.2	1.5	62	84	1.0
p7	4.0	44	0.72	Octahedra	2-Pyramid tetra	0	48.7	134.8	92.4	80.4	2.8	1.0	59	81	1.3
p8	3.8	43	0.72	Octahedra	2-Pyramid tetra	0	67.7	153.2	24.6	103.7	2.3	0.9	66	91	1.3
p9	3.8	43	0.72	Octahedra	2-Pyramid tetra	0	60.0	117.5	20.7	87.6	2.0	0.5	51	71	1.2
p10	4.8	46	0.74	Octahedra	2-Pyramid tetra	0	46.0	125.0	11.6	75.4	2.7	1.6	64	87	3.6
Mean PHe[g]: 82.7 $\pm$ 7.6 Ma, 9.2% deviation															
Published age: no published age for this location															
SA12-8A: Frank Smith Kimberlite															
p6	2.3	51	0.74	Dodecahedron	Elispoid	0	107.0	906.0	27.1	319.9	8.5	8.5	94	127	1.8
p7	1.7	46	0.71	Dodecahedron	Elispoid	0	118.5	1223.2	26.4	405.9	10.3	7.8	91	128	2.0
p8	2.2	50	0.73	Dodecahedron	Elispoid	0	82.6	930.8	19.6	301.3	11.3	7.0	88	120	0.7
p9	3.1	56	0.76	Dodecahedron	Elipsoid	0	151.2	1311.3	160.3	459.4	8.7	15.5	114	146	12.5
p10	2.5	53	0.74	Dodecahedron	Elispoid	0	185.1	2490.8	228.6	770.5	13.5	17.3	90	118	1.7
Mean: 127.6 $\pm$ 11.3 Ma, 9% deviation															
Published age: 113.7 $\pm$ 0.9, Rb-Sr, *Smith et al.* [1985]															
SA11-31A: Gansfontein Kimberlite															
p6	24.1	90	N/A	Fragment	N/A	N/A	79.0	157.4	10.0	116.0	51.27	27.7	81	N/A	9.5
p7	*23.8*	*86*	*N/A*	*Fragment*	*N/A*	*N/A*	*71.1*	*1125.8*	*311.3*	*335.7*	*217.44*	*116.1*	*118*	*N/A*	*35.9*
p8	3.7	53	0.78	Fragment	N/A	N/A	137.31	109.86	13.9	163	0.8	4.9	68	N/A	0.8
p9	6.6	62	0.81	Fragment	N/A	N/A	122.34	66.43	11.7	138	0.5	8.1	73	N/A	1.1
p10	8.4	67	0.80	Fragment	N/A	N/A	170.82	5475.06	33.10	1457	32.1	125.1	84	N/A	6.3
Mean: 76.5 $\pm$ 7.3 Ma, 9.5% deviation (excluding p7)															
No published age															
SA12-3: Koffiefontein Kimberlite															
p9	1.5	44	0.70	Dodecahedron	Elipsoid	0	321.4	4833.8	972.5	1457.3	15.04	11.7	69	94	22.8
p10	1.4	45	0.69	Dodecahedron	Elipsoid	0	213.1	3264.2	60.3	980.2	15.32	7.7	67	93	4.2
p11	3.1	50	N/A	Fragment	N/A	N/A	174.6	4631.9	159.0	1263.1	26.5	38.8	81	N/A	4.3
p12	1.8	42	N/A	Fragment	N/A	N/A	209.4	4302.1	25.8	1220.4	20.5	20.1	73	N/A	4.3
p13	1.6	40	N/A	Fragment	N/A	N/A	159.8	1489.7	30.6	509.9	9.3	6.7	68	N/A	3.3
Mean: 81.8 $\pm$ 11.6 Ma, 14.1% deviation															
Published age: 90.4, U-Pb zircon, *Davis et al.* [1977]															
SA11-33A: Melton Wold Kimberlite															
p6	12.3	79	N/A	Fragment	N/A	N/A	52.9	2214.9	6.0	573	41.9	141.1	164	N/A	7.5
p7	5.1	59	N/A	Fragment	N/A	N/A	24.1	1082.2	9.6	278	44.8	31.1	179	N/A	10.0
p8	5.7	62	N/A	Fragment	N/A	N/A	49.3	3076.7	10.5	772	62.4	81.5	151	N/A	3.0
p9[h]	13.4	82	N/A	Fragment	N/A	N/A	39.0	2114.3	13.7	536	54.0	149.7	170	N/A	26.9
p10[h]	2.2	45	N/A	Fragment	N/A	N/A	66.3	3351.3	137.7	854	50.5	40.9	176	N/A	46.3
Mean: 168.0 $\pm$ 11.0 Ma, 6.6% deviation															
Published age: 163 $\pm$ 2 Ma, *Griffin et al.* [2014]															
SA11-16A: Monastery Kimberlite															
p6	5.2	54	0.85	Cubic	0-Pyramid tetra	3	128.3	1596.1	190.9	503.3	12.4	26.0	81	95	16.9
p7	3.7	48	0.84	Cubic	0-Pyramid tetra	3	117.7	925.4	112.6	335.1	7.9	12.2	80	94	17.9
p8	3.4	47	N/A	Fragment	N/A	N/A	280.0	8209.6	249.0	2209.3	29.3	30.39	76	N/A	4.7
p9	2.0	35	N/A	Fragment	N/A	N/A	261.4	2112.6	30.7	757.9	8.1	8.47	90	N/A	1.4
p10	2.4	39	0.84	Cubic	0-Pyramid tetra	3	171.4	1415.4	35.0	504.0	8.3	5.37	70	84	1.4
Mean: 87.8 $\pm$ 7.9 Ma, 9.0% deviation															
Published age: 88.6 $\pm$ 1.1,U-Pb perovskite, *Batumike et al.* [2008]															
SA13-23: Olivine melilitite near Vaalputs															
p1	1.5	39	0.69	Fragment	N/A	N/A	82.0	269.8	39.4	145.5	3.3	1.1	42	N/A	0.9
p2	1.5	39	0.68	Fragment	N/A	N/A	76.5	412.9	29.9	173.6	5.4	1.3	39	N/A	9.3
p4	2.4	45	0.73	Fragment	N/A	N/A	35.4	162.0	19.1	73.5	4.6	0.9	42	N/A	2.8
p5	3.6	52	0.75	Fragment	N/A	N/A	14.6	111.6	35.1	40.8	7.6	0.8	46	N/A	2.7
Mean PHe: 42.0 $\pm$ 2.8 Ma, 6.8% deviation															
Published age: no published age for this location															

[a]Equivalent spherical radius, the radius of a sphere with the same surface area to volume ratio.
[b]Ft is α-ejection correction based on the geometries of *Ketcham et al.* [2011], see text for more detail.
[c]Observed grain shape.
[d]Approximated grain geometry used to calculate α-ejection correction based on *Ketcham et al.* [2011].
[e]eU, effective uranium concentration, weights U and Th for their alpha productivity, computed as [U] + 0.235 $\times$ [Th].
[f]Analytical uncertainty based on U, Th, He, and grain length measurements.
[g]Mean and 1σ standard deviation include the corrected dates for analyses with an α-ejection correction and the raw dates for those with no correction. Grains in italics not included.
[h]Grains used in diffusion experiments.

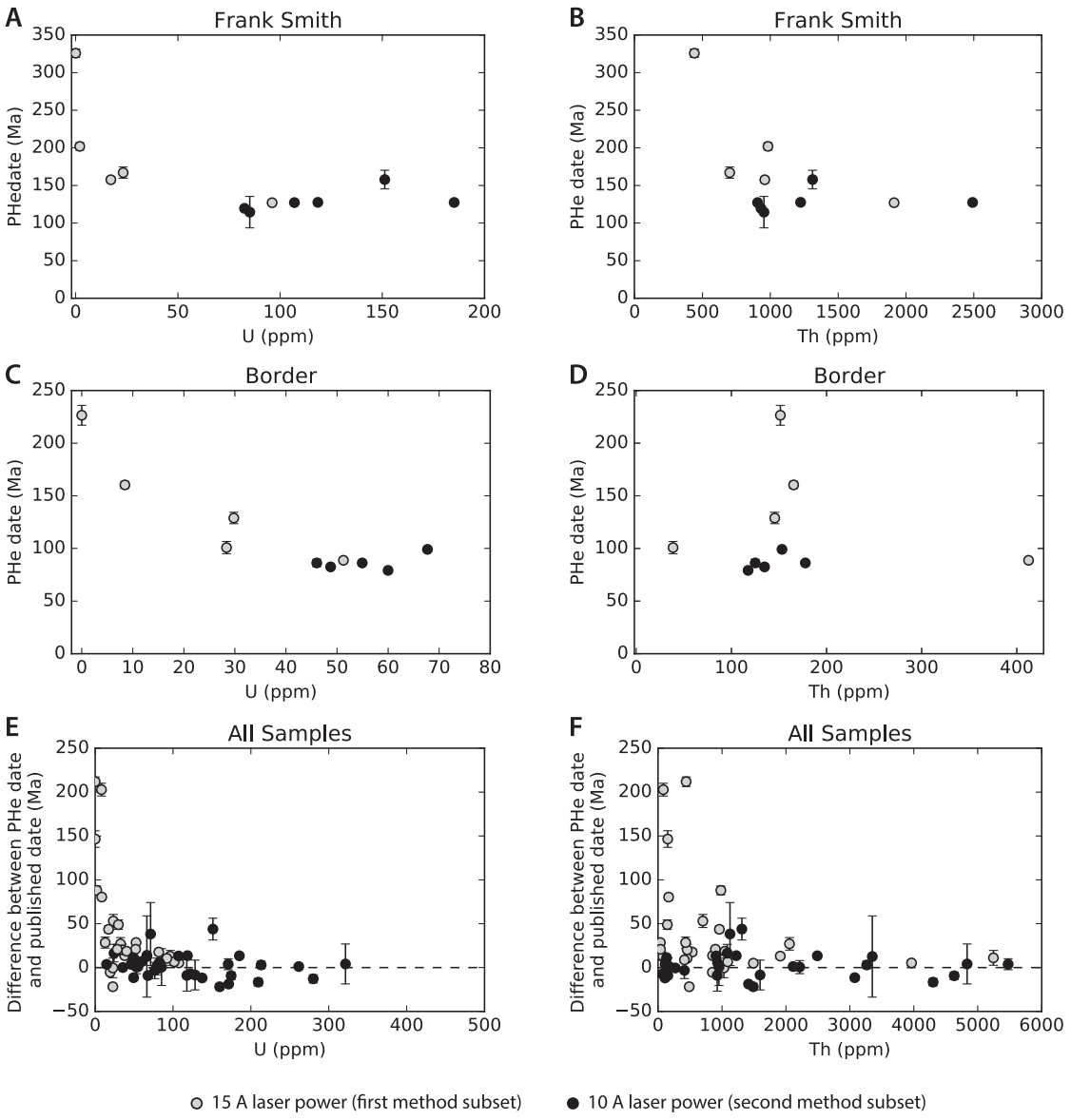

Figure 2. Comparison of PHe results generated by from the two analytical methods, where results acquired by the first method are in gray, and those by the preferred, modified method are in black. Individual PHe dates and 1σ analytical uncertainties for the Frank Smith kimberlite versus (a) U concentration and (b) Th concentration. (c, d) The same plots for the Border kimberlite. Difference between individual PHe date and the published kimberlite emplacement age versus (e) U concentration and (f) Th concentration for all samples. The expected date for each kimberlite is based on the published date (Table 1). Expected dates: Frank Smith 114 Ma, Monastery 89 Ma, Koffiefontein 90 Ma, Melton Wold 163 Ma, Gansfontein 75 Ma, Border 80 Ma, and Vaalputs 42 Ma.

patterns exhibited by multiple diffusion domain materials (e.g., He in hematite) [*Farley and Flowers*, 2012] but also could be caused by anisotropy (e.g., He in rutile) [*Cherniak and Watson*, 2011] or mineral inclusions. These initial steps comprise $<$1.5% of the total ^{4}He gas. The initial prograde sequence in ^{4}He diffusion experiments commonly lie off the main Arrhenius trend and is generally excluded from kinetic parameter calculation [e.g., *Guenthner et al.*, 2013]. Excluding the initial prograde steps, we used a standard linear regression to calculate kinetic parameters. The regressions yield values for the activation energy (E_a) of 351.7 $\pm$ 16.3 and 305.9 $\pm$ 12.7 kJ/mol, and log frequency factors (log D_0/a^2) of 13.0 $\pm$ 1.15 and 10.4 $\pm$ 0.93. These data are fit well by the linear regressions ($r^2 = 0.94$ and 0.97, respectively), suggesting that the gas was released by volume diffusion. The relationship between the Arrhenius trends for the larger grain ($r_s = 82$ μm) and smaller grain ($r_s = 45$ μm) suggest that the diffusion domain may be the size of the grain (supporting information Figure S3), but additional experiments on other size fractions are needed to

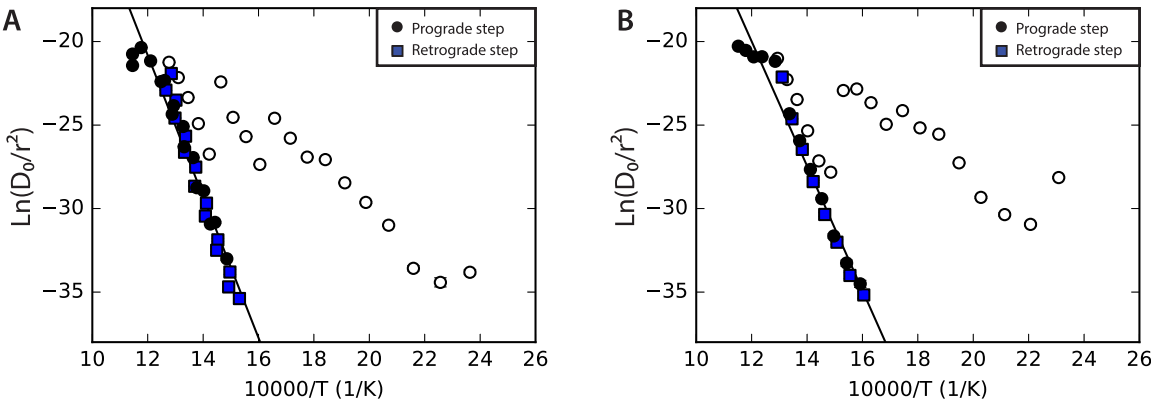

Figure 3. Arrhenius plots for two ^{4}He stepwise degassing experiments on individual Melton Wold kimberlite perovskite grains. (a) Grain p9 with 82 μm equivalent spherical radius and (b) grain p9 with 45 μm equivalent spherical radius. All error bars are smaller than the symbols and were calculated from the propagated uncertainty from the measured gas at each step. Black symbols are steps included in the linear regression used to calculated kinetic parameters. White symbols denote the initial prograde steps, which were discarded from the regression.

confirm this. The kinetic parameters derived from the best fit line on the Arrhenius plot (Figure 3) suggest closure temperatures of 377 +57/−53°C and 349 +49/−46°C, calculated using a spherical geometry and a cooling rate of 10°C/Ma [*Dodson*, 1973]. However, we were only able to release 5.6% and 6.6% of the total gas using the light bulb heating apparatus on our diffusion cell (supporting information Table S2). The difficulty of extracting the gas, as well as the Arrhenius regressions, are consistent with a high PHe closure temperature of >300°C. We emphasize that diffusion studies of additional perovskite crystals with greater gas release are required to fully characterize the He diffusion kinetics of this mineral.

5. Discussion

5.1. Comparison of ZHe Results With Published Ages

Of the seven kimberlites that yielded abundant zircon and reproducible ZHe dates, six had previously published emplacement ages. In five of those six cases, the ZHe date agrees with the published eruption age (Table 2). Figure 4 plots the mean ZHe dates and their 1σ uncertainties, along with the published emplacement dates also at the 1σ uncertainty level. All uncertainties are at the 1σ level unless otherwise stated. Koffiefontein and Klipfontein are closely related pipes that yielded mean ZHe dates of 92 ± 6 and 87 ± 13 Ma, respectively, which are consistent with their ~90–100 Ma zircon and perovskite U-Pb dates [*Davis*, 1977; *Griffin et al*., 2014]. Monastery yielded a mean ZHe date of 99 ± 4.5 Ma that overlaps within 2σ uncertainty the published perovskite U-Pb, zircon U-Pb, and Rb-Sr dates of 88–90 Ma. Letseng's mean ZHe date of 93 ± 3 Ma agrees well with a U-Pb zircon age of 94.6 [*Allsopp et al*., 1989]. We obtained a mean ZHe date of 102 ± 7 Ma for Liqhobong, which is slightly older than its U-Pb perovskite age of 91.2 ± 1 Ma [*Griffin et al*., 2014] but overlaps it at the 2σ uncertainty level.

One of our samples, Newlands, yielded reproducible ZHe dates (N = 5) with a mean value of 144 ± 12 Ma that is older than its published mica-whole-rock Rb-Sr isochron date of 114 ± 1 Ma [*Smith et al*., 1985] (Table 2). However, the ZHe result is in good agreement with the oldest apatite (U-Th)/He cooling dates of 115–144 Ma from this same sample [*Stanley et al*., 2015]. Newlands is a Group 2 kimberlite and the ZHe date is within the expected age range for kimberlites with Group 2 compositions, whereas its Rb-Sr result is slightly younger than many pipes of this group. We therefore favor our ZHe result as dating Newlands' emplacement age, and suggest that the Rb-Sr isochron was perturbed by post emplacement alteration or contamination of the whole rock Rb/Sr ratio.

The Koenaneng kimberlite is likely of Group 1 composition and has no published eruption age. This pipe and its dikes crosscut Karoo basalt dolerite dikes, indicating that the kimberlite is <183 Ma. Other Group 1 kimberlites nearby (Monastery and Letseng) have published eruption ages of ~90 Ma (see Table 1), so it is reasonable to expect that Koenaneng was erupted during the 100–80 Ma peak in Group 1 kimberlite magmatism. The six ZHe dates range from 81 to 250 Ma, but four of them cluster from 81 to 85 Ma with an average date of 82.7 ± 2 Ma that we interpret as the kimberlite's age. This kimberlite had two optically

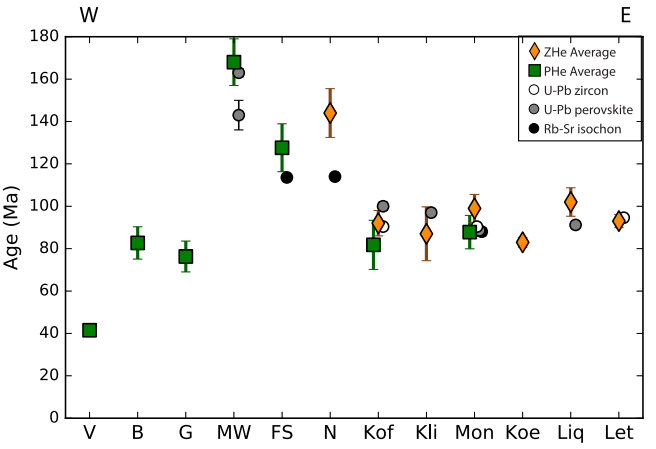

Figure 4. Average ZHe date and average PHe date along with published dates and 1σ uncertainties for studied kimberlites organized by latitude from west to east. Ages and references for published data are reported in Table 1. V: Vaalputs melilitite, B: Border, G: Gansfontein, MW: Melton Wold, FS: Frank Smith, N: Newlands, Kof: Koffiefontein, Kli: Klipfontein, Mon: Monastery, Koe: Koenaneng, Liq: Liqhobong, and Let: Letseng.

identifiable populations of zircon, and we infer that the two older outliers are from a xenocrystic population that was incompletely reset during eruption, as discussed further below.

Rietfontein was the only kimberlite studied with abundant zircon that did not yield reproducible results. (U-Th)/He dates for individual zircon ranged from 125 to 531 Ma. Rietfontein has two published eruption ages that disagree: a zircon U-Pb date of 71.9 Ma [*Davis*, 1977] and a perovskite U-Pb date of 135 $\pm$ 4.5 Ma [*Griffin et al.*, 2014]. The dispersed ZHe dates of this sample all overlap with or are older than these published ages.

The three zircon-poor kimberlites (<10 zircon in the separate) were unsuccessful at dating kimberlite eruption. Leicester has published zircon and perovskite U-Pb eruption dates of ~93 Ma (Table 1) [*Davis*, 1977; *Griffin et al.*, 2014]. The average ZHe date of 90 $\pm$ 32 Ma agrees with the published age, but has large dispersion (36%) so that the average is not meaningful (Table 2B). In addition to being scarce, the Leicester zircon grains have low U (<3 ppm) and Th ($\leq$15 ppm). Very low U minerals are especially susceptible to age bias due to α-particle implantation from nearby U-Th rich phases or the effects of U rich coatings [*Spiegel et al.*, 2009; *Gautheron et al.*, 2012; *Murray et al.*, 2014]. We attribute the dispersion in the low U-Th Leicester zircon dates to this same phenomenon.

Makganyene yielded individual ZHe dates that vary from 82 to 445 Ma, in contrast with this pipe's published mica Rb-Sr date of 121 $\pm$ 0.5 Ma [*Brown et al.*, 1989]. Loxtondal has no published eruption age, but it is a Group 2 kimberlite that crosscuts Karoo dolerite dikes [*Field and Scott Smith*, 1999] and therefore must be younger than ~183 Ma [*Svensen et al.*, 2012]. Most Group 2 kimberlites from southern Africa erupted before ~110 Ma [*Moore et al.*, 2008], so Loxtondal is probably older than 110 Ma. It is difficult to evaluate if any of the ZHe results from Loxtondal, which range from 10 to 258 Ma, date eruption.

5.2. ZHe Dating of Kimberlite Emplacement

Most of our samples with abundant zircon yielded reproducible dates consistent with published results, but several samples did not. Zircon is a relatively rare, late crystallizing phase in kimberlites that is generally characterized by very low U (<40 ppm) and Th (<10 ppm) concentrations [*Ahrens et al.*, 1967; *Belousova et al.*, 2002]. The ample zircon in the majority of our samples and their moderate to high U (30–2200 ppm) and Th (17–340 ppm) concentrations indicate that most dated zircon are likely xenocrystic rather than crystallizing directly from the kimberlite. The single exception to this pattern is Leicester, which yielded few zircon with very low U (<3 ppm) and Th ($\leq$15 ppm) concentrations, consistent with a kimberlitic origin.

Xenocrystic ZHe dates should accurately record kimberlite eruption in two circumstances. If the zircon resided at temperatures >200°C prior to eruption, equivalent to depths of ~8–10 km, then they would not accumulate He until entrainment and eruption in the kimberlite magma. In this case, the ZHe dates should be equivalent to the eruption date, assuming no resetting by younger events. Alternatively, if the zircon were at temperatures low enough for He accumulation prior to eruption, heating during the eruptive process could cause complete He loss and reset the (U-Th)/He system. Again, in this case the ZHe dates should be the kimberlite emplacement age if not perturbed at a later time. The majority of our ZHe results date kimberlite eruption and therefore the zircon likely underwent one of these histories. Eruption temperatures for most kimberlites appear to be >400°C [*Pell et al.*, 2015] but have been documented as low as ~150°C [*Stasiuk et al.*, 1999]. We suspect that the zircon with older He dates from Makganyene, Rietfontein, Loxtondal, and Koenaneng were derived from shallow enough depths for He accumulation prior to

entrainment, and then were incompletely degassed during eruption, perhaps due to incorporation late in the eruptive process.

In contrast, we interpret that the ZHe dates younger than eruption are a consequence of substantial radiation damage accumulation that lowered the temperature sensitivity of the dated grains. Radiation damage is generally thought to anneal at temperatures hotter than those required for He loss. If a zircon resided in the crust at cool enough temperatures for damage accumulation and then was not annealed during eruption, the zircon could have substantially lower He retentivity than annealed or undamaged zircon. For example, the youngest ZHe date from Loxtondal (10 Ma) is for a zircon with high eU (>3000 ppm). Such a high-eU zircon, if it retained damage from its preeruptive history, can have its temperature for ^{4}He retention lowered to <50°C [*Guenthner et al*., 2013]. Posteruption erosion of the kimberlites in this region has been documented with apatite (U-Th)/He thermochronology [*Stanley et al*., 2013, 2015], and we infer that these highly damaged zircon record this postemplacement erosion event. ZHe dates younger than kimberlite emplacement were also reported for a granitic xenolith from a Kansas kimberlite [*Blackburn et al*., 2008]. We suggest that those results can similarly be explained by high damage accumulation in the xenocrystic zircon such that their ZHe dates record posteruption near-surface processes.

In practice, we suggest that dating clear zircon with little damage (rather than hazy, brown, and fractured grains indicative of high damage) should largely avoid the problems above. Such grains are more likely to have been annealed during eruption or resided at temperatures too high for damage accumulation prior to eruption. We also advise dating a sufficient number of grains (at least five) to assess whether multiple age populations are present, and to interpret dispersed results with caution. In our study, samples that yielded few (<10) zircon were scattered, so it is preferable to avoid dating samples with negligible zircon yield. ZHe dates from kimberlites that experienced substantial burial and erosion, especially those from old (pre-Cretaceous) kimberlites where grains have had time to accumulate radiation damage, may record postemplacement processes and therefore represent a minimum kimberlite eruption age.

5.3. Comparison of PHe Results With Published Ages

Four of the seven kimberlites dated by PHe have published emplacement ages, as plotted in Figure 4. The mean PHe dates overlap the published ages within the 1σ uncertainty level for three of the four samples. Melton Wold's average PHe date of 168 ± 11 Ma is in good agreement with a recently published perovskite LA-ICP-MS U-Pb date of 163 ± 2 Ma [*Griffin et al*., 2014], though slightly older than the previously published perovskite SIMS U-Pb date (143 ± 14 Ma) [*Smith et al*., 1994]. Monastery yielded a mean PHe date of 88 ± 8 Ma, in good agreement with published perovskite U-Pb, zircon U-Pb, and Rb-Sr dates from 88 to 90 Ma [*Allsopp and Barrett*, 1975; *Davis*, 1977; *Batumike et al*., 2008]. It also overlaps within uncertainty our ZHe date of 99 ± 7 Ma for the same sample.

The average PHe date for Koffiefontein is 83 ± 12 Ma, overlaps within uncertainty our ZHe date of 92 ± 6 for this sample, and is consistent with a published zircon U-Pb date of 90.4 [*Davis*, 1977]. We dated both fragments and euhedral grains from this sample, all similarly sized and relatively small. The fragment PHe dates are somewhat younger (68–81 Ma) than those for the α-ejection corrected euhedral grains (93–94 Ma). The latter overlap well with the ZHe dates from this sample. One possible explanation for this pattern is that the fragments experienced α-ejection from grain portions near crystal faces, such that their uncorrected dates are too young. However, we cannot make an accurate α-ejection correction for the fragments without knowing their original crystal geometries. This potential problem would be less significant for larger fragments, or for small fragments from samples with large perovskite crystals such that the fragments are less likely to capture an exterior region of the grain affected by α-ejection.

Frank Smith, a transitional/Group 1 kimberlite located close to Newlands (Figure 1b), yields an average PHe age of 128 ± 11 Ma, which is slightly older that the published Rb-Sr isochron age of 114 ± 1 Ma [*Smith et al*., 1985], although it still overlaps at the 2σ level. Interestingly, both the average PHe date for Frank Smith and the average ZHe date for Newlands are older than the published Rb-Sr ages [*Smith et al*., 1985]. These two kimberlites are geographically close to one another and traditionally thought to be approximately the same age, despite their different compositions [*Smith et al*., 1985; *Field et al*., 2008]. Our ZHe and PHe dates suggest that perhaps both these pipes might be older than previously realized.

Gansfontein has no published date but yields a reproducible PHe date of 77 ± 7. Gansfontein is an off-craton kimberlite of Group 1 composition and is constrained to be <183 Ma based on its intrusion through the Karoo Supergroup. It is commonly considered to be similar in age to the petrographically similar nearby Hebron (also known as Hartbeesfontein) with a published Rb-Sr isochron age of 74.6 ± 0.6 Ma [*Smith et al*., 1994]. Our PHe date for Gansfontein is therefore reasonable.

The samples from the western portion of the study area, the Border kimberlite and a melilitite near the Vaalputs disposal site, lack published ages. The Border kimberlite is part of the Warmbad or Ariamsvlei kimberlite province with only a few published eruption ages from ~60 to 540 Ma (perovskite U-Pb0 [*Griffin et al*., 2014]. Our 83 ± 8 Ma PHe date for Border fits in this age span and is within the magmatism peak for the Group 1 kimberlites [*Jelsma et al*., 2004; *Moore et al*., 2008]. The undated melilitite near Vaalputs is part of the Bushmanland cluster with a few dated melilitites from 54 to 77 Ma based on whole rock K/Ar and zircon U-Pb analyses [*Davis*, 1977; *Moore and Verwoerd*, 1985; *Jelsma et al*., 2009]. Our melilitite PHe date of 42 ± 3 Ma is younger than these published emplacement ages for the cluster and suggests that the volcanism in this region continued for longer than previously thought.

5.4. PHe Dating of Kimberlite Emplacement

Generally, we found the PHe dates to be reproducible at ≤15% dispersion (1σ), consistent with previously published kimberlite eruption dates, and in agreement with our ZHe dates for the same pipes. Perovskite is a common groundmass mineral in kimberlites, and because it is uncommon in crustal rocks it is unlikely to be xenocrystic [*Kramers and Smith*, 1983]. Our preliminary diffusion experiments indicate that perovskite has a relatively high He closure temperature (>300°C) and therefore is less sensitive to posteruption events than zircon, although PHe dates for kimberlites that underwent substantial burial and erosion still have the potential to be reset and thus could represent a minimum kimberlite age. Additional diffusion experiments on perovskite grains of different composition and size are required to more fully constrain PHe diffusion kinetics. We recommend analysis of moderate to large perovskite grains and fragments (>35 μm equivalent spherical radius, or >60 μm minimum dimension) to minimize the uncertainty associated with the α-ejection correction.

6. Conclusions

We dated a suite of kimberlites from the Archean Kaapvaal Craton and its surrounding Proterozoic belts using ZHe (N = 11) and PHe (N = 7). Southern Africa has one of the most widely dated kimberlite suites worldwide, allowing us to assess the reliability of ZHe and PHe for dating kimberlites. ZHe dates were characterized by ≤15% dispersion in most samples with abundant zircon, most samples had <10% dispersion, and most were in good agreement with previously published ages. Nearly all the dated zircon were xenocrystic. We infer that zircons yielding reproducible dates either were at >200°C before eruption or were heated sufficiently during eruption to completely reset the (U-Th)/He system. A few of our samples had greater data dispersion, probably because shallowly sourced zircon accumulated He and radiation damage during the preeruptive history. These grains can yield ZHe dates older than the kimberlite if the zircon underwent incomplete He loss during eruption. Alternatively, these zircons can be younger than eruption if they were not annealed during the eruptive process, are highly radiation damaged, and have a lowered temperature sensitivity such that their He dates are more likely to be affected by posteruption events. We suggest that these potential problems can be circumvented by (1) avoiding grains that appear hazy, brown, or fractured and therefore are more likely to be highly radiation damaged, (2) dating only samples with abundant zircon, (3) dating sufficient zircon (at least 5) to detect whether multiple age populations are present, and (4) not interpreting ZHe data with substantial dispersion.

All samples with PHe dates were characterized by ≤15% dispersion (most <10% dispersion) and are in reasonable agreement with previously published dates. The PHe dates are consistent with but are generally more reproducible than, ZHe dates for the same sample. Our preliminary ^{4}He stepwise degassing experiments suggest a perovskite closure temperature >300°C, indicating that in many circumstances PHe dates should record the kimberlite eruption age rather than posteruption events. Because PHe is sensitive to higher temperatures than zircon and unlikely to be xenocrystic it may be more reliable than ZHe for dating kimberlite eruption. Perovskite grains should be degassed at lower temperatures than zircon during analysis

to avoid potential problems with U-Th volatilization. If the mineral assemblage allows, dating the kimberlite with both PHe and ZHe is a good strategy.

Kimberlites that experienced substantial burial and erosion since eruption have the potential to record post-emplacement near-surface processes, rather than the age of kimberlite eruption. In these cases the ZHe and PHe dates provide a minimum eruption age. The ZHe system is more vulnerable to posteruption resetting than PHe because zircon has a lower closure temperature (<200°C) than perovskite (>300°C), and zircon's He retentivity is reduced dramatically with increasing damage accumulation. As with any geochronologic data, it is important to interpret ZHe and PHe dates in the context of the geologic setting.

Typical uncertainties for the (U-Th)/He system are 10-15%, and therefore kimberlite ZHe and PHe dates are unlikely to achieve the same level of precision as high-precision U-Pb techniques. However, He dating is a relatively low-cost and time-efficient method that may be preferred in circumstances where high-precision dates are not required. PHe dating may also prove effective for determining the actual kimberlite emplacement age if multiple age populations are observed in an U-Pb perovskite data set [i.e., *Heaman*, 1989; *Griffin et al*., 2011]. Thus, PHe and ZHe dating can be valuable complementary techniques to current methods.

Acknowledgments

This work was supported by NSF EAR-0951518 and EAR-1126991 to R.M.F. and a NSF Graduate Research Fellowship to J.R.S. All data supporting our conclusions can be found in Tables 2 and 3 in the main text and Tables S2 and S3 in the supporting information. We thank John Gurney and Steve Richardson at the University of Cape Town for access to samples from the Mantle Room collection and Marco Andreoli for access to the Vaalputs site. We also thank Sebastian Tappe, Ferdi Winters, and Andrew Webster at De Beers; Bob Burrell at Letseng Diamonds; and Sentle Hlajoane for assistance with kimberlite sample acquisition. Many thanks to David Bell, Maarten de Wit, Jock Robey, Jay Barton, Lew Ashwal, and Sue Webb for insightful discussions. We appreciate the help and support of Maria Shipapo and Warren Miller during fieldwork. We thank Jim Metcalf for analytical assistance with (U-Th)/He work. Willy Guenthner, Andy Moore, Sebastian Tappe, and an anonymous reviewer provided insightful comments that helped improve the manuscript.

References

Ahrens, L. H., R. D. Cherry, and A. J. Erlank (1967), Observations on the Th-U relationship in zircons from granitic rocks and from kimberlites, *Geochim. Cosmochim. Acta*, *31*(12), 2379–2387.

Allsopp, H. L., and D. R. Barrett (1975), Rb-Sr age determinations on South African kimberlite pipes, *Phys. Chem. Earth*, *9*, 605–617.

Allsopp, H. L., J. W. Bristow, C. B. Smith, R. Brown, A. J. W. Gleadow, J. D. Kramers, and O. G. Garvie (1989), A summary of radiometric dating methods applicable to kimberlites and related rocks, in *Proceedings of the Fourth international Kimberlite Conference*, vol. 1, pp. 343–357, Geol. Soc. of Aust. Carlton, Perth, Australia.

Appleyard, C. M., D. R. Bell, and A. P. Roex (2007), Petrology and geochemistry of eclogite xenoliths from the Rietfontein kimberlite, Northern Cape, South Africa, *Contrib. Mineral. Petrol.*, *154*(3), 309–333, doi:10.1007/s00410-007-0195-7.

Ault, A. K., and R. M. Flowers (2012), Is apatite U–Th zonation information necessary for accurate interpretation of apatite (U–Th)/He thermochronometry data?, *Geochim. Cosmochim. Acta*, *79*, 60–78.

Batumike, J. M., W. L. Griffin, E. A. Belousova, N. J. Pearson, S. Y. O'Reilly, and S. R. Shee (2008), LAM-ICPMS U-Pb dating of kimberlitic perovskite: Eocene-Oligocene kimberlites from the Kundelungu Plateau, D.R. Congo, *Earth Planet. Sci. Lett.*, *267*(3–4), 609–619, doi:10.1016/j.epsl.2007.12.013.

Becker, M., and A. P. Le Roex (2006), Geochemistry of South African on-and off-craton, Group I and Group II kimberlites: Petrogenesis and source region evolution, *J. Petrol.*, *47*(4), 673–703.

Becker, M., A. P. Le Roex, and C. Class (2007), Geochemistry and petrogenesis of South African transitional kimberlites located on and off the Kaapvaal Craton, *S. Afr. J. Geol.*, *110*(4), 631–646, doi:10.2113/gssajg.110.4.631.

Bell, D. R., M. D. Schmitz, and P. E. Janney (2003), Mesozoic thermal evolution of the southern African mantle lithosphere, *Lithos*, *71*(2–4), 273–287, doi:10.1016/S0024-4937(03)00117-8.

Belousova, E., W. Griffin, S. Y. O'Reilly, and N. Fisher (2002), Igneous zircon: Trace element composition as an indicator of source rock type, *Contrib. Mineral. Petrol.*, *143*(5), 602–622, doi:10.1007/s00410-002-0364-7.

Blackburn, T. J., D. F. Stockli, R. W. Carlson, and P. Berendsen (2008), (U–Th)/He dating of kimberlites—A case study from north-eastern Kansas, *Earth Planet. Sci. Lett.*, *275*(1–2), 111–120, doi:10.1016/j.epsl.2008.08.006.

Blondes, M. S., P. W. Reiners, B. R. Edwards, and A. Biscontini (2007), Dating young basalt eruptions by (U-Th)/He on xenolithic zircons, *Geology*, *35*(1), 17–20, doi:10.1130/G22956A.1.

Brown, R. W., H. L. Allsoppl, J. W. Bristow, and C. B. Smith (1989), Improved precision of Rb-Sr dating of kimberlitic micas: An assessment of a leaching technique, *Chem. Geol. Isotope Geosci. Sect.*, *79*(2), 125–136.

Brown, R. W., R. Beucher, S. Roper, C. Persano, F. Stuart, and P. Fitzgerald (2013), Natural age dispersion arising from the analysis of broken crystals. Part I: Theoretical basis and implications for the apatite (U–Th)/He thermochronometer, *Geochim. Cosmochim. Acta*, *122*(120), 478–497, doi:10.1016/j.gca.2013.05.041.

Chalapathi Rao, N. V., A. Dongre, F. Y. Wu, and B. Lehmann (2015), A Late Cretaceous (ca. 90 Ma) kimberlite event in southern India: Implication for sub-continental lithospheric mantle evolution and diamond exploration, *Gondwana Res.*, *35*, 373–398, doi:10.1016/j.gr.2015.06.006.

Cherniak, D. J., and E. B. Watson (2011), Helium diffusion in rutile and titanite, and consideration of the origin and implications of diffusional anisotropy, *Chem. Geol.*, *288*(3–4), 149–161, doi:10.1016/j.chemgeo.2011.07.015.

Cox, R. A., and D. H. C. Wilton (2006), U-Pb dating of perovskite by LA-ICP-MS: An example from the Oka carbonatite, Quebec, Canada, *Chem. Geol.*, *235*(1–2), 21–32, doi:10.1016/j.chemgeo.2006.06.002.

Currie, C. A., and C. Beaumont (2011), Are diamond-bearing Cretaceous kimberlites related to low-angle subduction beneath western North America?, *Earth Planet. Sci. Lett.*, *303*(1–2), 59–70, doi:10.1016/j.epsl.2010.12.036.

Davis, G. L. (1977), The ages and uranium contents of zircons from kimberlites and associated rocks, *Carnegie Inst. Wash. Yearb.*, *76*, 631–654.

Dawson, J. B. (1962), Basutoland Kimberlites, *Geol. Soc. Am. Bull.*, *73*, 545–560.

Dodson, M. H. (1973), Closure temperature in cooling geochronological and petrological systems, *Contrib. Mineral. Petrol.*, *40*(3), 259–274.

Duke, G. I., R. W. Carlson, C. D. Frost, B. C. Hearn, and G. N. Eby (2014), Continent-scale linearity of kimberlite–carbonatite magmatism, mid-continent North America, *Earth Planet. Sci. Lett.*, *403*, 1–14, doi:10.1016/j.epsl.2014.06.023.

Ehlers, T. A. (2005), Crustal thermal processes and the interpretation of thermochronometer data, *Rev. Mineral. Geochemistry*, *58*, 315–350, doi:10.2138/rmg.2005.58.12.

Farley, K. A., and R. M. Flowers (2012), (U–Th)/Ne and multidomain (U–Th)/He systematics of a hydrothermal hematite from eastern Grand Canyon, *Earth Planet. Sci. Lett.*, *359*, 131–140.

Farley, K. A., R. A. Wolf, and L. T. Silver (1996), The effects of long alpha-stopping distances on (U-Th)/He ages, *Geochim. Cosmochim. Acta*, *60*(21), 4223–4229.
Farley, K. A., P. W. Reiners, and V. Nenow (1999), An apparatus for high precision helium diffusion measurements from minerals, *Anal. Chem.*, *71*(10), 2059–2061.
Farley, K. A., D. L. Shuster, and R. A. Ketcham (2011), U and Th zonation in apatite observed by laser ablation ICPMS, and implications for the (U–Th)/He system, *Geochim. Cosmochim. Acta*, *75*(16), 4515–4530.
Fechtig, H., and S. Kalbitzer (1966), The diffusion of argon in potassium-bearing solids, in *Potassium Argon Dating*, pp. 68–107, Springer, Berlin Heidelberg.
Field, M., and B. H. Scott Smith (1999), Contrasting geology of near-surface emplacement of kimberlite pipes in southern Africa and Canada, in *Proceedings of the Seventh International Kimberlite Conference*, edited by J. J. Gurney, pp. 214–237, Red Roof Design, Cape Town, South Africa.
Field, M., J. Stiefenhofer, J. Robey, and S. Kurszlaukis (2008), Kimberlite-hosted diamond deposits of southern Africa: A review, *Ore Geol. Rev.*, *34*(1–2), 33–75, doi:10.1016/j.oregeorev.2007.11.002.
Flowers, R. M., and S. A. Kelley (2011), Interpreting data dispersion and "inverted" dates in apatite (U–Th)/He and fission-track datasets: An example from the US midcontinent, *Geochim. Cosmochim. Acta*, *75*(18), 5169–5186, doi:10.1016/j.gca.2011.06.016.
Flowers, R. M., D. L. Shuster, B. P. Wernicke, and K. A. Farley (2007), Radiation damage control on apatite (U-Th)/He dates from the Grand Canyon region, Colorado Plateau, *Geology*, *35*(5), 447, doi:10.1130/G23471A.1.
Flowers, R. M., R. A. Ketcham, D. L. Shuster, and K. A. Farley (2009), Apatite (U–Th)/He thermochronometry using a radiation damage accumulation and annealing model, *Geochim. Cosmochim. Acta*, *73*(8), 2347–2365, doi:10.1016/j.gca.2009.01.015.
Gautheron, C., and L. Tassan-Got (2010), A Monte Carlo approach to diffusion applied to noble gas/helium thermochronology, *Chem. Geol.*, *273*(3–4), 212–224, doi:10.1016/j.chemgeo.2010.02.023.
Gautheron, C., L. Tassan-Got, J. Barbarand, and M. Pagel (2009), Effect of alpha-damage annealing on apatite (U–Th)/He thermochronology, *Chem. Geol.*, *266*(3), 157–170.
Gautheron, C., L. Tassan-Got, R. A. Ketcham, and K. J. Dobson (2012), Accounting for long alpha-particle stopping distances in (U–Th–Sm)/He geochronology: 3D modeling of diffusion, zoning, implantation, and abrasion, *Geochim. Cosmochim. Acta*, *96*, 44–56.
Griffin, W. (2003), The evolution of lithospheric mantle beneath the Kalahari Craton and its margins, *Lithos*, *71*(2–4), 215–241, doi:10.1016/j.lithos.2003.07.006.
Griffin, W. L., G. C. Begg, D. Dunn, S. Y. O'Reilly, L. M. Natapov, and K. Karlstrom (2011), Archean lithospheric mantle beneath Arkansas: Continental growth by microcontinent accretion, *Geol. Soc. Am. Bull.*, *123*(9–10), 1763–1775.
Griffin, W. L., J. M. Batumike, Y. Greau, N. J. Pearson, S. R. Shee, and S. Y. O'Reilly (2014), Emplacement ages and sources of kimberlites and related rocks in southern Africa: U–Pb ages and Sr–Nd isotopes of groundmass perovskite, *Contrib. Mineral. Petrol.*, *168*(1), 1032, doi:10.1007/s00410-014-1032-4.
Guenthner, W. R., P. W. Reiners, R. A. Ketcham, L. Nasdala, and G. Giester (2013), Helium diffusion in natural zircon: Radiation damage, anisotropy, and the interpretation of zircon (U-TH)/He thermochronology, *Am. J. Sci.*, *313*(3), 145–198, doi:10.2475/03.2013.01.
Haggerty, S. E., E. Raber, and C. W. Naeser (1983), Fission track dating of kimberlitic zircons, *Earth Planet. Sci. Lett.*, *63*(1), 41–50, doi:10.1016/0012-821X(83)90020-1.
Heaman, L. M. (1989), The nature of the subcontinental mantle from Sr Nd Pb isotopic studies on kimberlitic perovskite, *Earth Planet. Sci. Lett.*, *92*(3), 323–334.
Heaman, L. M., and B. A. Kjarsgaard (2000), Timing of eastern North American kimberlite magmatism: Continental extension of the Great Meteor hotspot track?, *Earth Planet. Sci. Lett.*, *178*(3), 253–268.
Heaman, L. M., B. A. Kjarsgaard, and R. A. Creaser (2004), The temporal evolution of North American kimberlites, *Lithos*, *76*(1), 377–397.
Helmstaedt, H., and J. J. Gurney (1984), Kimberlites of southern Africa—Are they related to subduction processes, *Kimberlites*, *1*, 424–438.
Janney, P. E., S. B. Shirey, R. W. Carlson, D. G. Pearson, D. R. Bell, A. P. Le Roex, A. Ishikawa, P. H. Nixon, and F. R. Boyd (2010), Age, composition and thermal characteristics of South African off-Craton mantle lithosphere: Evidence for a multi-stage history, *J. Petrol.*, *51*(9), 1849–1890, doi:10.1093/petrology/egq041.
Jelsma, H., W. Barnett, S. Richards, and G. Lister (2009), Tectonic setting of kimberlites, *Lithos*, *112*, 155–165, doi:10.1016/j.lithos.2009.06.030.
Jelsma, H. A., M. J. de Wit, C. Thiart, P. H. G. M. Dirks, G. Viola, I. J. Basson, and E. Anckar (2004), Preferential distribution along transcontinental corridors of kimberlites and related rocks of Southern Africa, *S. Afr. J. Geol.*, *107*, 301–324.
Johnstone, S., J. Hourigan, and C. Gallagher (2013), LA-ICP-MS depth profile analysis of apatite: Protocol and implications for (U–Th)/He thermochronometry, *Geochim. Cosmochim. Acta*, *109*, 143–161, doi:10.1016/j.gca.2013.01.004.
Ketcham, R. A., C. Gautheron, and L. Tassan-Got (2011), Accounting for long alpha-particle stopping distances in (U-Th-Sm)/He geochronology: Refinement of the baseline case, *Geochim. Cosmochim. Acta*, *75*(24), 7779–7791, doi:10.1016/j.gca.2011.10.011.
Kobussen, A. F., W. L. Griffin, S. Y. O'Reilly, and S. R. Shee (2008), Ghosts of lithospheres past: Imaging an evolving lithospheric mantle in southern Africa, *Geology*, *36*(7), 515, doi:10.1130/G24868A.1.
Kramers, J. D., and C. B. Smith (1983), A feasibility study of U−Pb and Pb−Pb dating of kimberlites using groundmass mineral fractions and whole-rock samples, *Chem. Geol.*, *41*, 23–38.
Le Roex, A. P. (1986), Geochemical correlation between southern African kimberlites and South Atlantic hotspots, *Nature*, *324*(6094), 243–245.
LeCheminant, A. N., L. M. Heaman, U. Kretschmar, and P. C. LeCouteur (1998), Complex origin and multiple ages of mantle zircon megacrysts from Canadian and South African kimberlites, in *Extended Abstracts, 7th International Kimberlite Conference*, edited by J. J. Gurney, pp. 486–488, Red Roof Design, Cape Town, South Africa.
Li, Q. L., X. H. Li, Y. Liu, F. Y. Wu, J. H. Yang, and R. H. Mitchell (2010), Precise U-Pb and Th-Pb age determination of kimberlitic perovskites by secondary ion mass spectrometry, *Chem. Geol.*, *269*(3–4), 396–405, doi:10.1016/j.chemgeo.2009.10.014.
McCandless, T. E. (1999), Kimberlites: Mantle expressions of deep-seated subduction, in *Proceedings of the 7th international Kimberlite Conference*, vol. 2, edited by J. J. Gurney, pp. 545–549, Red Roof Design, Cape Town, South Africa.
Moore, A., and E. Belousova (2005), Crystallization of Cr-poor and Cr-rich megacryst suites from the host kimberlite magma: Implications for mantle structure and the generation of kimberlite magmas, *Contrib. Mineral. Petrol.*, *149*(4), 462–481.
Moore, A., T. Blenkinsop, and F. (Woody) Cotterill (2008), Controls on post-Gondwana alkaline volcanism in Southern Africa, *Earth Planet. Sci. Lett.*, *268*(1–2), 151–164, doi:10.1016/j.epsl.2008.01.007.
Moore, A. E., and W. J. Verwoerd (1985), The olivine melilitite-"kimberlite"-carbonatite suite of Namaqualand and Bushmanland, South Africa, *Trans. Geol. Soc. S. Afr.*, *88*, 281–294.

Murray, K. E., D. A. Orme, and P. W. Reiners (2014), Effects of U–Th-rich grain boundary phases on apatite helium ages, *Chem. Geol.*, *390*, 135–151, doi:10.1016/j.chemgeo.2014.09.023.

Nowell, G. M., D. G. Pearson, D. R. Bell, R. W. Carlson, C. B. Smith, P. D. Kempton, and S. R. Noble (2004), Hf isotope systematics of kimberlites and their megacrysts: New constraints on their source regions, *J. Petrol.*, *45*(8), 1583–1612.

Pell, J., J. K. Russell, and S. Zhang (2015), Kimberlite emplacement temperatures from conodont geothermometry, *Earth Planet. Sci. Lett.*, *411*, 131–141, doi:10.1016/j.epsl.2014.12.003.

Phillips, D., G. B. Kiviets, E. S. Barton, C. B. Smith, K. S. Viljoen, and L. F. Fourie (1999), $^{40}Ar/^{39}Ar$ dating of kimberlites and related rocks: Problems and solution, in *Proceedings of the 7th International Kimberlite Conference, Cape Town, South Africa*, vol. 2, edited by J. J. Gurney, pp. 677–688, Red Roof Design, Cape Town, South Africa.

Reiners, P. W. (2005), Zircon (U-Th)/He thermochronometry, *Rev. Mineral. Geochem.*, *58*(1), 151–179.

Reiners, P. W., and K. A. Farley (1999), Helium diffusion and (U–Th)/He thermochronometry of titanite, *Geochim. Cosmochim. Acta*, *63*(22), 3845–3859, doi:10.1016/S0016-7037(99)00170-2.

Reiners, P. W., and K. A. Farley (2001), Influence of crystal size on apatite (U-Th)/He thermochronology: An example from the Bighorn Mountains, Wyoming, *Earth Planet. Sci. Lett.*, *188*, 413–420, doi:10.1016/S0012-821X(01)00341-7.

Reiners, P. W., and D. L. Shuster (2009), Thermochronology and landscape evolution, *Phys. Today*, *62*, 31–36.

Sarkar, C., L. M. Heaman, and D. G. Pearson (2015), Duration and periodicity of kimberlite volcanic activity in the Lac de Gras kimberlite field, Canada and some recommendations for kimberlite geochronology, *Lithos*, *218 219–*, 155–166, doi:10.1016/j.lithos.2015.01.017.

Shuster, D. L., and K. A. Farley (2009), The influence of artificial radiation damage and thermal annealing on helium diffusion kinetics in apatite, *Geochim. Cosmochim. Acta*, *73*(1), 183–196.

Shuster, D. L., R. M. Flowers, and K. A. Farley (2006), The influence of natural radiation damage on helium diffusion kinetics in apatite, *Earth Planet. Sci. Lett.*, *249*, 148–161, doi:10.1016/j.epsl.2006.07.028.

Skinner, E. M. W. (1989), Contrasting Group I and Group II kimberlite petrology: Towards a genetic model for kimberlites, *Kimberlites Relat. Rocks*, *1*, 528–544.

Skinner, E. M. W., C. B. Smith, K. S. Viljoen, and T. C. Clark (1992), The petrography, tectonic setting and emplacement ages of kimberlites in the south western border region of the Kaapvaal Craton, Prieska area, South Africa, in *Kimberlites, Related Rocks and Mantle Xenoliths, Proceedings of the 5th International Kimberlite Conference, CPRM*, pp. 80–97, Spec. Publ., Brasilia.

Smith, C. B. (1983), Pb, Sr and Nd isotopic evidence for sources of southern African Cretaceous kimberlites, *Nature*, *304*, 51–54, doi:10.1038/304051a0.

Smith, C. B., H. L. Allsopp, J. D. Kramers, G. Hutchinson, and J. C. Roddick (1985), Emplacement ages of Jurassic-Cretaceous South African kimberlites by the Rb-Sr method on phlogopite and whole-rock samples, *Trans. Geol. Soc. S. Afr.*, *88*, 249–266.

Smith, C. B., T. C. Clark, E. S. Barton, and J. W. Bristow (1994), Emplacement ages of kimberlite occurrences in the Prieska region, southwest border of the Kaapvaal Craton, South Africa, *Chem. Geol.*, *113*(1–2), 149–169, doi:10.1016/0009-2541(94)90010-8.

Spiegel, C., B. Kohn, D. Belton, Z. Berner, and A. Gleadow (2009), Apatite (U–Th–Sm)/He thermochronology of rapidly cooled samples: The effect of He implantation, *Earth Planet. Sci. Lett.*, *285*(1), 105–114.

Stanley, J. R., R. M. Flowers, and D. R. Bell (2013), Kimberlite (U-Th)/He dating links surface erosion with lithospheric heating, thinning, and metasomatism in the southern African Plateau, *Geology*, *41*, 1243–1246, doi:10.1130/G34797.1.

Stanley, J. R., R. M. Flowers, and D. R. Bell (2015), Erosion patterns and mantle sources of topographic change across the southern African Plateau derived from the shallow and deep records of kimberlites, *Geochem. Geophys. Geosyst.*, *16*, 3235–3256, doi:10.1002/2015GC005969.

Stasiuk, L. D., G. D. Lockhart, W. W. Nassichuk, and J. A. Carlson (1999), Thermal maturity evaluation of dispersed organic matter inclusions from kimberlite pipes, Lac de Gras, Northwest Territories, Canada, *Int. J. Coal Geol.*, *40*(1), 1–25, doi:10.1016/S0166-5162(98)00053-6.

Svensen, H., F. Corfu, S. Polteau, Ø. Hammer, and S. Planke (2012), Rapid magma emplacement in the Karoo large igneous province, *Earth Planet. Sci. Lett.*, *325*, 1–9.

Tagami, T., K. A. Farley, and D. F. Stockli (2003), (U-Th)/He geochronology of single zircon grains of known Tertiary eruption age, *Earth Planet. Sci. Lett.*, *207*(1–4), 57–67, doi:10.1016/S0012-821X(02)01144-5.

Tappe, S., and A. Simonetti (2012), Combined U-Pb geochronology and Sr-Nd isotope analysis of the Ice River perovskite standard, with implications for kimberlite and alkaline rock petrogenesis, *Chem. Geol.*, *304 305–*, 10–17, doi:10.1016/j.chemgeo.2012.01.030.

Tappe, S., B. A. Kjarsgaard, S. Kurszlaukis, G. M. Nowell, and D. Phillips (2014), Petrology and Nd-Hf isotope geochemistry of the neoproterozoic amon kimberlite sills, Baffin Island (Canada): Evidence for deep mantle magmatic activity linked to supercontinent cycles, *J. Petrol*, 55(10), 2003–2042, doi:10.1093/petrology/egu048.

Tappe, S., N. B. Brand, A. Stracke, D. van Acken, C.-Z. Liu, H. Strauss, F.-Y. Wu, A. Luguet, and R. H. Mitchell (2016), Plates or plumes in the origin of kimberlites: U/Pb perovskite and Sr-Nd-Hf-Os-CO isotope constraints from the Superior craton (Canada), *Chem. Geol.*, doi:10.1016/j.chemgeo.2016.08.019, in press.

Torsvik, T. H., K. Burke, B. Steinberger, S. J. Webb, and L. D. Ashwal (2010), Diamonds sampled by plumes from the core-mantle boundary, *Nature*, *466*(7304), 352–355, doi:10.1038/nature09216.

Torsvik, T. H., R. Van Der Voo, P. V. Doubrovine, K. Burke, B. Steinberger, L. D. Ashwal, R. G. Trønnes, S. J. Webb, and A. L. Bull (2014), Deep mantle structure as a reference frame for movements in and on the Earth, *Proc. Natl. Acad. Sci. U. S. A.*, *111*(24), 201318135, doi:10.1073/pnas.1318135111.

Woodhead, J., J. Hergt, D. Phillips, and C. Paton (2009), African kimberlites revisited: In situ Sr-isotope analysis of groundmass perovskite, *Lithos*, *112*, 311–317, doi:10.1016/j.lithos.2009.03.031.

Wu, F.-Y., Y.-H. Yang, R. H. Mitchell, Q.-L. Li, J.-H. Yang, and Y.-B. Zhang (2010), In situ U–Pb age determination and Nd isotopic analysis of perovskites from kimberlites in southern Africa and Somerset Island, Canada, *Lithos*, *115*(1–4), 205–222, doi:10.1016/j.lithos.2009.12.010.

Ziegler, J. F., M. D. Ziegler, and J. P. Biersack (2010), SRIM–The stopping and range of ions in matter, *Nucl. Instruments Methods Phys. Res. Sect. B Beam Interact. with Mater. Atoms,* 268, 1818–1823.